Arch. Min. Sci. **71** (2026), 1, 123-142

Electronic version (in color) of this paper is available: http://mining.archives.pl

DOI: https://doi.org/10.24425/ams.2026.157759

LICHAO CHENG[1*], LEI LI[1], XINWANG LI[1], LEI DI[2], SHOUJIAN PENG[3], DAMING YANG[1], YUNDE HAO[1], ZHENRUI LI[1]

ANALYSIS OF FLOOR STABILITY UNDER THE COUPLED INFLUENCE OF MINING-INDUCED DISTURBANCE AND CONFINED WATER

This study investigates floor stability in underground coal mining, considering the coupled effects of backfilling and confined aquifer pressure. Using a North China coal mine's 9101 fully mechanised mining face as a case study, a formula for maximum floor failure depth under confined water pressure was derived using the zero-position failure principle and superposition. A numerical model was developed to analyse how vertical stress, permeability, porosity, and pore water pressure in the floor evolve with varying backfill rates. The interrelationship of these parameters at different floor locations was analysed to determine how backfilling impacts the effective impermeable layer thickness and overall floor stability. Results show the theoretical formula accurately predicts the plastic zone height; increasing mining face advancement increases maximum vertical stress, but this stress negatively correlates with backfill rate; higher backfill rates reduce permeability (up to 45%); at 120 m advancement, the increased porosity zones in the caving method aquiclude and the Ordovician aquifer show a connection, but higher backfill rates significantly reduce overall porosity; increased backfill rates lower pore water pressure, reducing the plastic zone and confined water rise; floor stress and permeability are negatively correlated, while porosity increases due to mining; and the water inrush face experienced both pore water pressure increase and recovery zones. This research provides a theoretical foundation for safely mining coal above deep confined aquifers.

Keywords: Fill mining; Pressurized water; Base Plate; Stability analysis

[1] HEBEI UNIVERSITY OF ENGINEERING, HANDAN TECHNOLOGY INNOVATION CENTER FOR LARGE-SCALE UTILIZATION OF COAL BASED SOLID WASTE, HANDAN, HEBEI 056038, CHINA

[2] TECHNICAL PLANNING DEPARTMENT, XINGTAI MINE, JIZHONG ENERGY CO., LTD., XINGTAI, HEBEI 054000, CHINA

[3] STATE KEY LABORATORY OF COAL MINE DISASTER DYNAMICS AND CONTROL, CHONGQING UNIVERSITY, CHONGQING 400044, CHINA

* Corresponding author: chenglichao169@163.com

1. Introduction

The stability of the floor is a key issue faced by mining above confined water [1-3]. Research on the stability of the floor under the influence of mining and confined water coupling has important theoretical significance and application value [4-8].

At present, domestic and foreign experts and scholars have conducted a lot of research on the stability of the floor above confined water. In terms of theoretical research, Sun W. et al. [9] studied the characteristics of floor damage caused by mining and confined water, and proposed that the evolution of the water inrush channel in the mining floor can be divided into three stages: floor crack development stage, water channel manifestation stage and channel evolution stage. Liu Jiangong et al. [10-11] conducted research on the problem of safe coal mining above confined water in the Handan-Xingxing mining area and believed that when the elastic modulus of the filling body increased to 50MPa, no instability expansion would occur, and the inhibitory effect of the filling body and the destructive effect of the confined water reached a state of equilibrium. In terms of similar simulations, Li Z. et al. [12] proposed an innovative fluid-solid coupling experimental model to simulate the interaction between fluid and solid in the coal seam floor. The model aims to reflect the fluid-solid coupling characteristics in the actual coal seam floor so as to more accurately analyse the mechanism of the water inrush process. In terms of numerical modelling, Lu Y. et al. [13] used the finite element method (FEM) and discrete element method (DEM) to study the evolution of cracks in the coal seam floor caused by mine pressure during mining and its interaction with the water flow in the confined aquifer. It reveals how geological changes caused by coal mining affect groundwater flow and provides a prediction method for the risk of water inrush in mines. It can be seen that there are many theoretical research results on the stability of the floor of the caving mining area, but there are few studies on the stability of the floor under the dual influence of filling mining and confined water, as well as the linkage relationship between vertical stress, permeability, porosity and pore water pressure at different positions of the floor.

This paper takes the 9101 working face of a mine in the North China coalfield as the research background, theoretically obtains the formula for the maximum depth of floor destruction in confined water mining, and systematically studies the evolution of vertical stress, permeability, porosity and pore water pressure of the floor of the filling mining working face with different filling rates as the filling rate changes. This analysis explores the relationship between vertical stress, permeability, porosity, and pore water pressure at various positions in the floor during mining. It examines how filling affects the thickness of the effective waterproof layer in the floor and enhances its waterproof stability. The research results lay a theoretical foundation for safe and water-saving mining of deep confined water coal resources.

2. Overview of engineering geological conditions

The 9101 comprehensive mining face of a mine in the North China coalfield is the first mining face of the 9100 mining area. The ground position is 30 m west of Binjiang Road and north of Xibeiliu Village. There are no lakes, rivers, or other surface water at the corresponding ground position, and the mining of the face will not be affected by surface water. The 9101 comprehensive mining face is located in the middle of the 9100 mining area underground, east

of the QF1 fault. There are no defects such as faults and sinkholes within the pre-mining range of the face, and the mining will not be affected by faults. To the south is the protective coal pillar line of Xibeiliu Village, to the west is the F6 fault, and to the north is 9100 for transporting waste rock up the mountain. The 9101 working face has a strike length of 200 m and an inclination length of 80m. It adopts a waste rock filling mining method. The average distance between the bottom plate of the working face and the Ordovician grey aquifer is 26 m. The ground elevation is +92.1～+92.7 m, and the working face elevation is –120～–140 m.

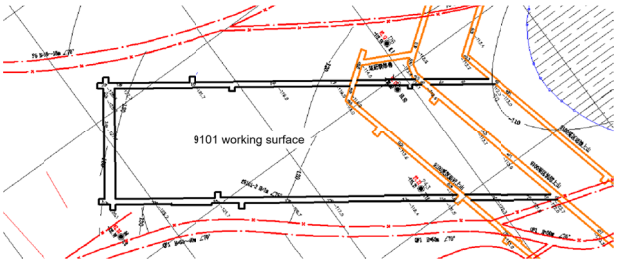

Fig. 1. General situation of 9101 working face in Xingtai Mine

3. Theoretical calculation of the maximum failure depth of the floor in confined water mining

3.1. Theoretical calculation of the maximum failure depth of the floor under the influence of mining

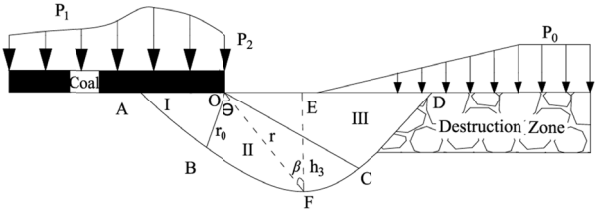

Fig. 2. Zero damage principle diagram

As shown in Fig. 2, some scholars proposed the zero-position failure theory of the mining floor [14]. The zero-position failure field of the floor is subjected to the pressure of the coal pillar in front of the goaf, forming a logarithmic spiral sliding plastic zone equation at the floor:

$$r = r_0 e^{\theta \tan \varphi} \tag{1}$$

In the formula, r is the distance between the coal wall O and the floor failure spiral curve BF; ro is the distance between OB; θ is the angle between OB and OF; and φ is the friction angle

of the floor rock. From the geometric relationship, it can be seen that the maximum depth of floor failure h [15-16] is

$$h = r\cos\beta \tag{2}$$

In the formula, β is the angle between the maximum damage depth line and OF. According to the geometric relationship, we can get:

$$\beta = \theta + \frac{\varphi}{2} - \frac{\pi}{4} \tag{3}$$

Assume that the width of the plastic zone of the coal wall OA is L [17], where γ is the bulk density of the coal rock mass; H is the buried depth of the coal seam; T is the inclined length of the working face; σ_t is the tensile strength of the coal rock mass; and K is the stress concentration coefficient.

$$L = \frac{(\gamma H)^2 TK}{256(\sigma_t)} \tag{4}$$

According to the geometric relationship, the side length of the Rankine active zone triangle can be obtained as r_0:

$$r_0 = \frac{L}{2\cos\alpha} \tag{5}$$

In summary, the expression of the bottom plate failure depth of the collapse method can be obtained:

$$h = \frac{(\gamma H)^2 TK}{512(\sigma_T)^2 \cos\left(\frac{\pi}{4} + \frac{\varphi}{2}\right)} e^{\theta\tan\varphi} \cdot \cos\left(\theta + \frac{\varphi}{2} - \frac{\pi}{4}\right) \tag{6}$$

Taking the first-order derivative of the above formula with respect to θ, we can conclude that when $\theta = \frac{\varphi}{2} + \frac{\pi}{4}$, the bottom plate waterproof layer reaches its maximum damage depth:

$$h_{\max} = \frac{(\gamma H)^2 TK}{512(\sigma_T)^2 \cos\left(\frac{\pi}{4} + \frac{\varphi}{2}\right)} e^{\left(\frac{\varphi}{2} + \frac{\pi}{4}\right)\tan\varphi} \cdot \cos\varphi \tag{7}$$

3.2. Theoretical calculation of bottom plate failure depth under the influence of confined water

During the mining process on confined water, the confined water will provide an upward hydrostatic pressure on the bottom plate. Ignoring the hydrodynamic pressure of the confined water, the bottom plate aquiclude can be equivalent to a fixed beam, and the confined water effect can be equivalent to an upward uniformly distributed load. Figs. 3(a) and 3(c) are the bottom plate aquiclude models for caving mining and solid filling mining, respectively.

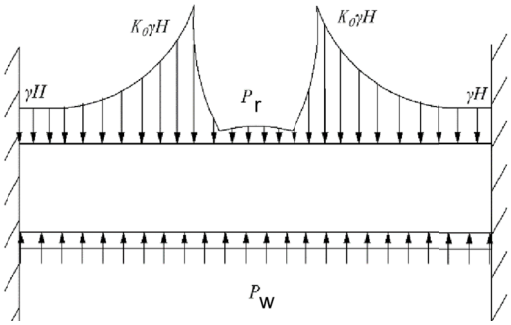

(a) Mechanical model of aquiclude mining by caving method

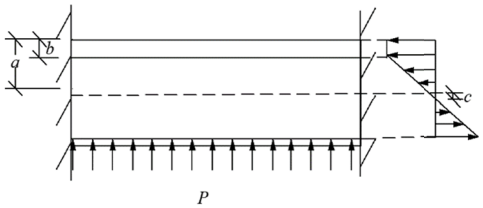

(b) Stress diagram of aquiclude under the influence of confined water during caving mining

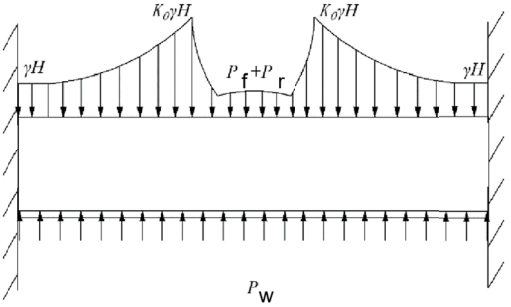

(c) Mechanical model of aquiclude in solid filling mining

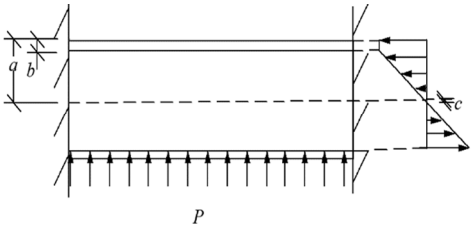

(d) Stress diagram of aquiclude under the influence of confined water in solid filling mining

Fig. 3. The mechanical model of the water-resistant layer for mining above confined water

The depth of floor damage caused by mining has been calculated, so only the depth of the floor plastic zone caused by confined water is calculated. Figs. 3(b) and 3(d) are the stress diagrams of the aquiclude under the influence of confined water, where *a* is half the thickness of

the aquiclude, *b* is the height of the plastic zone, and *c* is the offset distance of the neutral axis of the floor aquiclude before and after mining.

The bottom plate's waterproof layer produces an upward deflection after being subjected to the upward pressure of the pressurised water. The waterproof layer is in a state of compression at the bottom and tension at the top, and the tensile strength of the coal rock mass is much smaller than the compressive strength. Therefore, according to the force characteristics, the fixed-support beam suffers tensile failure in the middle of the span, and a plastic zone appears. The appearance of the plastic zone at the top of the waterproof layer causes the neutral axis to shift downward. The fixed-support beam span structure under uniform load exhibits the largest deflection at the midpoint of the span, which is also where the zone of plastic tensile cracking first appears.

From structural mechanics, it is known that the stress state of the mid-span section can be expressed as follows [18]:

$$\begin{cases} N_{Pressure} = \int_{c-a}^{0} \dfrac{\sigma_T\, y}{a+c-b}\, dy \\ N_{Pull} = \int_{0}^{a+c-b} \dfrac{\sigma_T\, y}{a+c-b}\, dy \\ N_{Plasticity} = b\sigma_T \\ M_{Pressure} = \int_{c-a}^{0} \dfrac{\sigma_T\, y^2}{a+c-b}\, dy \\ M_{Pull} = \int_{0}^{a+c-b} \dfrac{\sigma_T\, y^2}{a+c-b}\, dy \\ M_{Plasticity} = b\sigma_T \left(a+c-\dfrac{b}{2} \right) \end{cases} \Rightarrow \begin{cases} N_{Pressure} = \dfrac{\sigma_T}{2}(a+c-b) \\ N_{Pull} = \dfrac{\sigma_T (a-c)^2}{2(a+c-b)} \\ N_{Plasticity} = c\sigma_T \\ M_{Pressure} = \dfrac{\sigma_T (c-a)^3}{3(a+c-b)} \\ M_{Pull} = \dfrac{\sigma_T}{3}(a+c-b)^2 \\ M_{Plasticity} = b\sigma_T \left(a+c-\dfrac{b}{2} \right) \end{cases} \tag{8}$$

According to mechanics, the equilibrium equation is:

$$\begin{cases} M_{Pressure} + M_{Pull} + M_{Plasticity} = M_{\max} \\ N_{Pressure} + N_{Pull} + N_{Plasticity} = 0 \\ M_{\max} = \dfrac{ql^2}{8} \end{cases} \tag{9}$$

In summary, the height b of the plastic zone of the bottom plate aquiclude under the action of pressurised water can be calculated as:

$$b = \frac{ql^2}{8a\sigma_T} - a \tag{10}$$

From the above formula, we can see that the depth of plastic zone development is positively correlated with the strength of confined water, and negatively correlated with the thickness of the

effective impermeable layer and the tensile strength of the impermeable layer. Backfill mining can control the stress field of the floor to inhibit the rise of confined water and indirectly increase the thickness of the floor:

$$a_{Collapse} < a_{filling}$$

From this, we can deduce:

$$b_{Collapse} < b_{filling}$$

It can be seen that backfill mining can effectively inhibit the effect of confined water on the development of the floor plastic zone.

The formula for the floor failure depth caused by combined mining stress is obtained by the superposition method, and the formula for the maximum failure depth of the floor in confined water mining is:

$$h_{\max} = \frac{(\gamma H)^2 TK}{512(\sigma_T)^2 \cos\left(\frac{\pi}{4}+\frac{\varphi}{2}\right)} e^{\left(\frac{\varphi}{2}+\frac{\pi}{4}\right)\cdot\tan\varphi} \cdot \cos\varphi + \frac{ql^2}{8a\sigma_T} - a \tag{11}$$

The parameters of the 9101 working face of a mine in the North China coalfield were brought in, and the maximum damage depth was 12.46 m. The actual measurement was 13.3 m. The calculation formula had an error of 6.3%, which was more realistic. It can be seen that backfill mining can effectively reduce the floor damage depth under the coupling of mining and pressurised water, and improve the floor stability.

4. Construction of FLAC3D numerical simulation model

4.1. Model building

In order to better study the protection mechanism of the floor stability under the coupling of mining and confined water, a numerical model was established according to the geological conditions of a mine in the North China coalfield, as shown in Fig. 4. This simulation established a 400 m × 200 m × 180 m three-dimensional confined water mining numerical simulation model, which was divided into 198,400 units and 211,071 grid nodes.

The establishment and parameter selection of the model refer to the actual rock formation of the 9101 working face of a mine in the North China coalfield, see TABLE 1. The numerical simulation model in this paper does not simulate the surface, and the thickness of the rock formation which is not established in the upper part of the model, is 101 m. The rock formation bulk density is 2400, so the pressure applied on the upper surface of the model is $q = \sum \gamma h$ =2400 × 9.8 × 101 = 2.4 MPa. Sliding constraints were applied around the model, fixed constraints were applied at the bottom, and no constraints were applied at the top. A 2.6 MPa water pressure was fixed 30 m below the bottom plate to simulate constant pressure water. To facilitate subsequent simulations, 16 measuring points were arranged 3 m below the working surface, with a spacing of 12.5 m. The measuring points were numbered C1-C16.

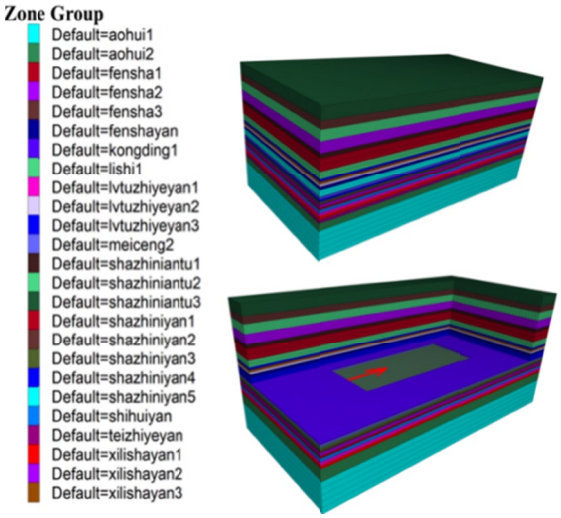

Fig. 4. Numerical simulation model diagram

TABLE 1

Numerical simulation parameters of rock strata

	Name	Thickness (m)	ρ kg·m^{-3}	E GPa	ν	φ °	c MPa	σ_t MPa
1	Ordovician limestone 1	40	2650	4.03	0.23	27.4	5.1	4.41
2	Ordovician limestone 2	10	2564	1.86	0.18	19.3	3.1	5.03
3	Ferruginous shale	5	2400	1.36	0.23	32.32	2.8	5.31
4	Fine-grained sandstone 1	4	2426	3.08	0.26	28.31	6.4	6.32
5	Aluminous shale 1	4	2400	1.36	0.23	32.32	2.6	5.31
6	Limestone	4	2579	1.64	0.16	19.54	3.2	5.02
7	Sandy mudstone 1	3	2494	3.34	0.28	28.21	2.3	2.48
8	Fine-grained sandstone 2	3	2426	3.08	0.26	28.31	6.4	6.32
9	Sandy mudstone 2	2	2579	1.64	0.16	19.54	2.1	5.02
10	Fine-grained sandstone 3	2	2426	3.08	0.26	28.31	6.4	6.32
11	Coal seam	3	2555	3.14	0.26	26.66	1.2	1.12
12	Sandy mudstone 3	8	2579	1.64	0.16	19.54	6.4	5.02
13	Siltstone	4	2579	1.64	0.16	19.54	4.8	5.02
14	Ordovician limestone 1	3	2400	1.36	0.23	32.32	2.4	5.31
15	Ordovician limestone 2	3	2426	3.08	0.26	28.31	4.26	6.32
16	Ferruginous shale	3	2400	1.36	0.23	32.32	2.4	5.31
17	Fine-grained sandstone 1	9	2450	7	0.28	35.02	0.2	0.45
18	Aluminous shale 1	15	2579	1.64	0.16	19.54	0.68	1.32
19	Limestone	5	2132	1.23	0.31	32.12	0.13	1.51
20	Sandy mudstone 1	13	2579	1.64	0.16	19.54	0.68	1.32
21	Fine-grained sandstone 2	12	2132	1.23	0.31	32.12	0.13	1.51
22	Sandy mudstone 2	11	2579	1.64	0.16	19.54	0.68	1.32
23	Fine-grained sandstone 3	15	2132	1.23	0.31	32.12	0.13	1.51

4.2. Fluid-Structure Interaction Equation

The coal rock mass is regarded as a continuous equivalent porous medium, and the water permeation migration in the pores is considered to conform to Darcy's law. Therefore, the fluid-solid coupling implementation of FLAC3D follows the following equation:

(1) Conduction equation

$$q_i = -k_\eta^a \frac{\partial}{\partial x}\left(P - \rho_w g_k x_k\right) \tag{12}$$

Where q_i is the relative flow vector; k_η^a is the liquidity coefficient.

(2) Balance equation

$$\frac{\partial \zeta}{\partial t} = -\frac{\partial q_i}{\partial x_i} + q_v \tag{13}$$

Where ζ is the change in fluid volume per unit volume of void material; and q_v is the volume flow source intensity.

(3) Constitutive equation

$$\frac{\partial P}{\partial t} = M\left(\frac{\partial \zeta}{\partial t} - \alpha \frac{\partial \varepsilon}{\partial t}\right) \tag{14}$$

Where M is the Biot modulus; a is the effective stress Biot coefficient; and ε is the volume strain.

Principle of effective stress of coal and rock mass under solid-solid coupling state:

$$\sigma' = \sigma + p \tag{15}$$

In the formula, σ' is the effective stress; and p is the pore water pressure.

Changes in effective stress in coal and rock mass will lead to changes in shear strength:

$$T = \mu \cdot \sigma' \tag{16}$$

Changes in pore water pressure can also affect seepage:

$$\frac{\Delta V}{V} = K_f \cdot \Delta P \tag{17}$$

4.3. Functional relationship between permeability and volumetric strain

Using the built-in FISH language of FLAC3D, the permeability formulas of different rock layers are edited separately, and the different permeability and volume strain function relationships are substituted into the corresponding rock layers to establish the relationship between the permeability and volume strain of each rock layer model, and then combined with the whilestep-

ping function to realise the dynamic change of the permeability of each rock layer. The following formula is the permeability and volume strain function relationship:

$$y = y_0 + \frac{A}{\omega\sqrt{\pi/2}} e^{-2\frac{(x-x_c)^2}{\omega^2}} \tag{18}$$

The permeability change cloud diagram is shown in Fig. 5. The coal walls on both sides of the goaf jointly bear the pressure of the overlying rock strata in the goaf and the compression of the floor below the coal walls, resulting in a decrease in permeability and the appearance of a "spoon-shaped" permeability reduction area. The floor is subjected to tension and shear, and plastic failure occurs, resulting in a "bowl-shaped" permeability increase area. The increase in the permeability of the aquiclude provides a good guide condition for the pressurised water.

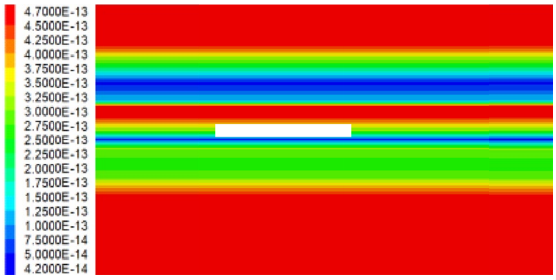

(a) Without considering the permeability change

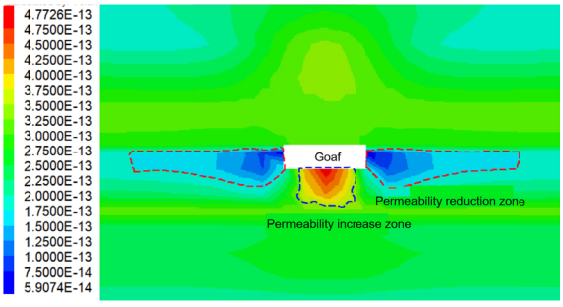

(b) Considering permeability changes

Fig. 5. Permeability changes in the surrounding rock of the base plate

4.4. Relationship between porosity and volume strain

Edit the porosity formula below into FISH language for secondary development of FLAC3D. This achieves the effect that the porosity of the floor surrounding rock changes with mining. This reduces the error of the numerical simulation software and is more in line with the actual project.

$$\phi = 1 - \frac{1-\phi_0}{1-\varepsilon_v} = \frac{\phi_0 + \varepsilon_v}{1-\varepsilon_v} \tag{19}$$

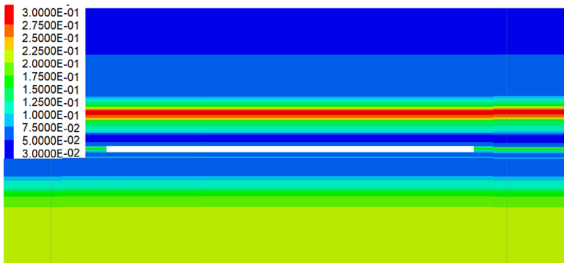

(a) No consideration of porosity changes

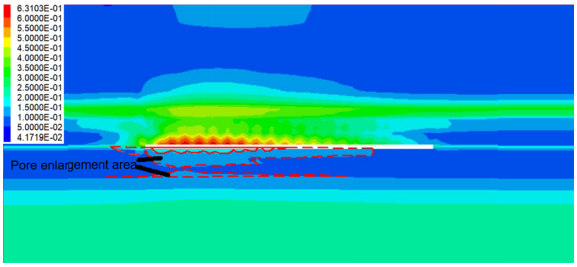

(b) Considering porosity variation

Fig. 6. Diagram of porosity change

The evolution law of the floor porosity in mining above confined water is shown in Fig. 6: When the floor is depressurised and expanded, the floor bulges along the plastic slip line under the extrusion of the coal wall, and a porosity increase zone appears in the floor aquiclude. The rock layer where the confined water is located produces an upward displacement under the action of lateral pressure. The change in volumetric strain leads to a change in porosity, which also produces a porosity increase zone in the water-bearing rock layer. As the working face advances, the two porosity increase zones will interpenetrate to form a porosity increase zone. At this point, the porosity of the aquiclude in this area has increased, providing good conditions for the lifting of confined water.

4.5. Simulation scheme

The mining face is 200 m long and 40 m wide, and is mined in steps. The Mohr-Coulomb model is used for the coal stratum, and the double yield model is selected for the filling body. The seepage field developed by the fish language is applied, and the mining process is 10 m each time.

5. Analysis of floor stability under different filling rates

5.1. Analysis of the influence of different filling rates on the bottom plate stress field

In order to study the influence of the caving method and different filling rates (70%, 80%, 90%) on the floor stress, the water pressure was maintained at 2.6 MPa, and the elastic modulus

of the filling body was maintained at 0.05 GPa. Numerical simulation calculations were performed, and the three-dimensional stress diagrams at the same distance from the working face with different filling rates were intercepted, and the line graphs of the changes in the peak value of the vertical stress under the conditions of different filling rates as the working face advances were drawn, as shown in Figs. 7 and 8.

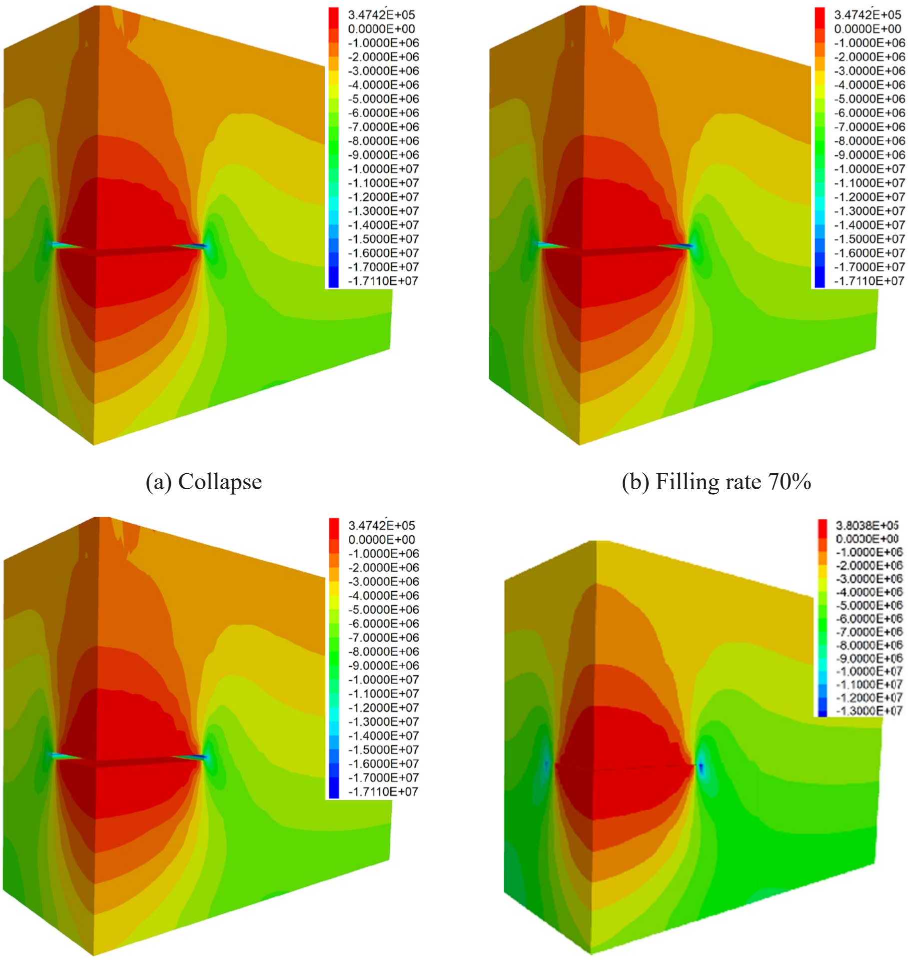

(a) Collapse (b) Filling rate 70%

(c) Filling rate 80% (d) Filling rate90%

Fig. 7. working face advancing 120 m stress distribution contrast chart

When the working face advances 120 m, stress concentration zones are formed in the coal walls in front of and behind the working face. The peak vertical stresses of caving mining and filling mining with different filling rates (70%, 80%, 90%) reach 17.1 MPa, 15.5 MPa, 13.6 MPa, and 13.0 MPa, respectively. This shows that filling mining can effectively reduce the peak vertical stress, and the higher the filling rate, the lower the peak stress. A pressure relief zone appears

below the goaf. And with the advancement of the working face, the scope of the pressure relief zone continues to expand, and the pressure relief zone extends to the confined aquifer, promoting water migration. The scope of the pressure relief zone decreases with the increase in the filling rate. With the increase in the mining advancement distance, the maximum vertical stress of the floor increases accordingly. In the early stage of mining, the maximum vertical stress increases rapidly. When the mining reaches 40 m, the maximum vertical stress of the floor slows down with the increase of mining depth, and the maximum vertical stress of the floor is negatively correlated with the filling rate.

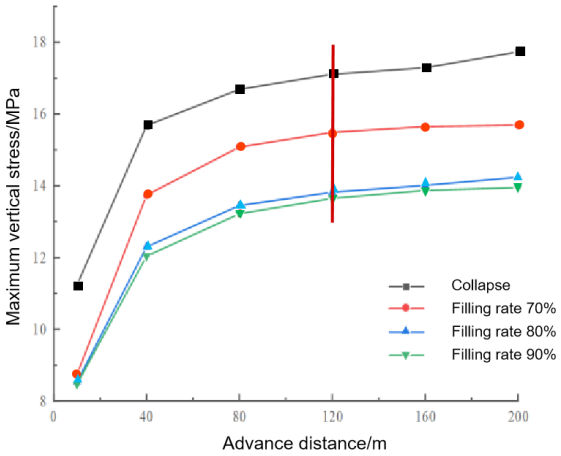

Fig. 8. The variation curve of vertical stress peak with advancing distance under different filling rates

5.2. Evolution of floor permeability under different filling rates

In order to explore the influence of different filling rates on the permeability under the floor, the permeability change diagrams of different filling rates and the same distance were intercepted, and the permeability change curve with the advancement of the working face was constructed by taking 5m under the floor as an example.

As can be seen from Figs. 9 and 10, due to mining disturbance, the roof of the goaf collapsed, and the floor broke. Therefore, the permeability of the top of the goaf increased the most, followed by the floor. The coal walls in front and behind the working face were affected by the disturbance, which led to the compression and closure of the rock cracks, blocking the formation of water-conducting channels. The permeability decreased, and the filling rate was positively correlated with the permeability of the front and rear coal walls. This study mainly considered the change in the permeability of the floor during the mining process. It can be seen from the simulation that the permeability of the floor is the highest in the collapse mining method, and the permeability area diverges from the floor to the bottom, showing a “bowl-shaped” trend. With the increase of the filling rate, the permeability gradually decreases, and the “bowl-shaped” divergence area of the permeability area decreases. When the filling rate reaches 90%, the permeability area almost disappears, that is, the filling mining with a high filling rate is conducive to the reduction of the porosity of the floor.

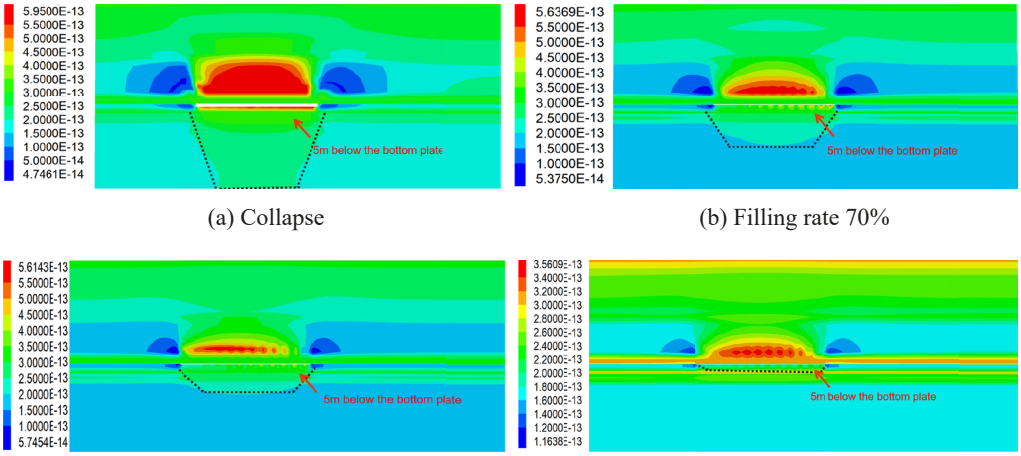

(a) Collapse (b) Filling rate 70%

(c) Filling rate 80% (d) Filling rate90%

Fig. 9. working face advancing 120 m permeability distribution contrast map

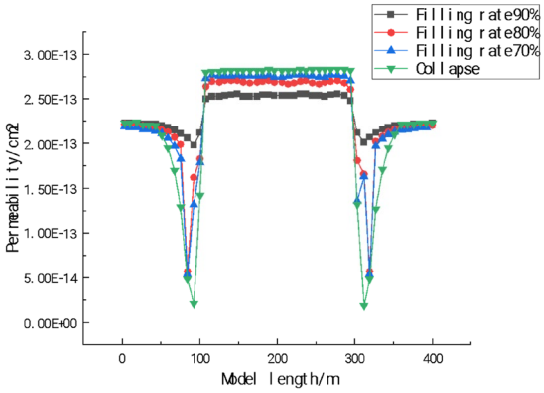

Fig. 10. The permeability distribution of 5 m under the floor at the end of mining

5.3. Analysis of floor porosity evolution under different filling rates

In order to study the influence of the caving method and different filling rates (70%, 80%, 90%) on the evolution of the porosity of the bottom plate, the confined water pressure was maintained at 2.6 MPa, and the elastic modulus of the filling body was 0.05 GPa. A simulation analysis was performed to intercept the porosity distribution cloud map at different advancement distances, as shown in Fig. 11.

As the working face advances, the porosity of the floor of the caving mining face increases, and the porosity of the upper impermeable layer of the Ordovician ash also increases. The rock strata in the upper and lower porosity increase areas tend to be conductive. When the working face advances to 120 m, the porosity increases. The area of the impermeable layer of the

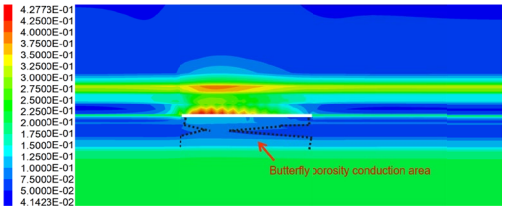

(a) Collapse

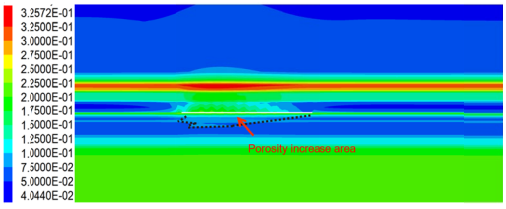

(b) Filling rate 70%

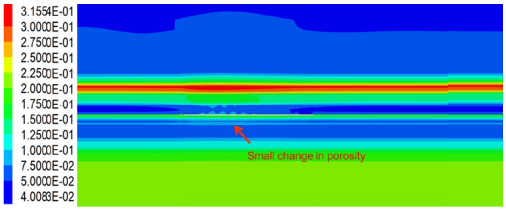

(c) Filling rate 80%

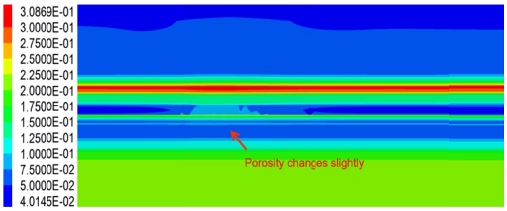

(d) Filling rate90%

Fig. 11. working face advancing 120 m porosity distribution contrast chart

caving working face develops laterally and coincides with the upper porosity increase area of the Ordovician ash aquifer, forming a “butterfly”-shaped porosity increase area, which provides spatial conditions for floor water inrush. As the filling rate of the goaf increases, the porosity change gradually decreases. In the early stage of mining, the surrounding rock of the floor is less disturbed, the porosity is basically unaffected, and the porosity of the filling mining working face remains basically unchanged. An area of increased porosity also appears below the working face with a filling rate of 70%, but this increased area is not conductive with the Ordovician ash

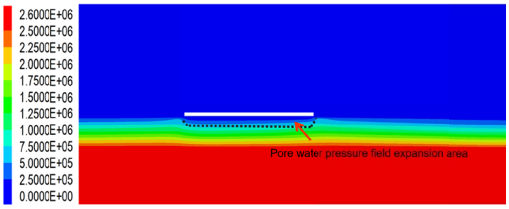

(a) Collapse

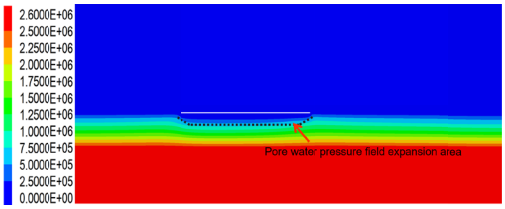

(b) Filling rate 70%

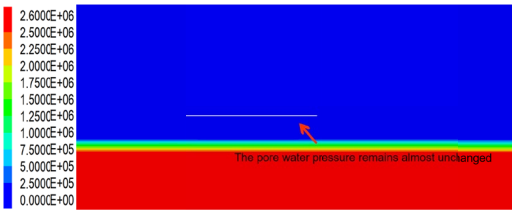

(c) Filling rate 80%

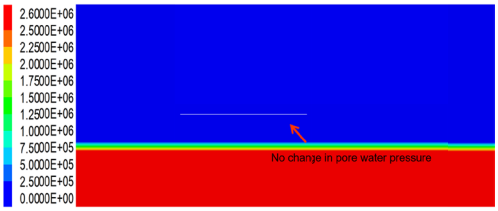

(d) Filling rate90%

Fig. 12. working face advancing 40 m hole pressure field distribution contrast chart

water. The porosity of the floor impermeable layer with a filling rate of 80% and a filling rate of 90% remains basically unchanged. It can be seen that filling mining can effectively control the porosity of the floor impermeable layer and improve the stability of the floor.

5.4. Analysis of the evolution characteristics of pore water pressure in the bottom plate under different filling rates

This section studies the variation of the pore water pressure in the bottom plate under the conditions of the caving method and different filling rates (filling rate 70%, filling rate 80%, filling rate 90%), maintaining the pressure of the confined water at 2.6 MPa and the filling body modulus at 0.05 GPa. A simulation study and analysis were conducted to obtain a cloud diagram of the variation of the pressure water conductivity during the solid filling mining process on the confined water at the same distance under different filling rates. As shown in Fig. 13.

The pore pressure field continues to rise upward as mining progresses. The pore pressure field on the floor on both sides of the goaf is high, and the pore pressure directly below the goaf is relatively low. When mining under the caving method and a filling rate of 70%, the pore water pressure field of the floor expands. After the pore pressure field rises to the floor, it is distributed in a bowl shape. Due to the existence of the water head difference, water will flow from the floor into the goaf. When mining under a filling rate of 80% and a filling rate of 90%, the confined water is lifted to a certain extent due to mining disturbance. However, the pore water pressure field eventually stabilises and has no expansion trend. Filling can effectively suppress the rise of confined water. The greater the filling rate, the smaller the rise speed of confined water and the smaller the final rise height.

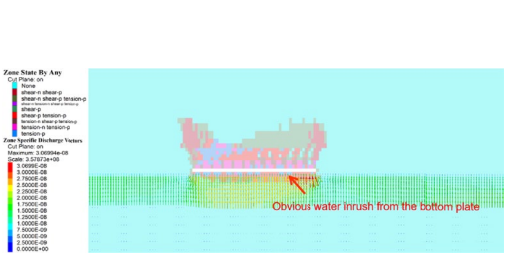

(a) Collapse

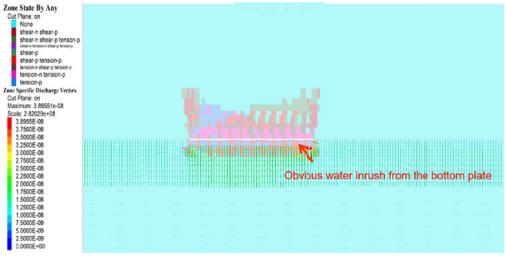

(b) Filling rate 70%

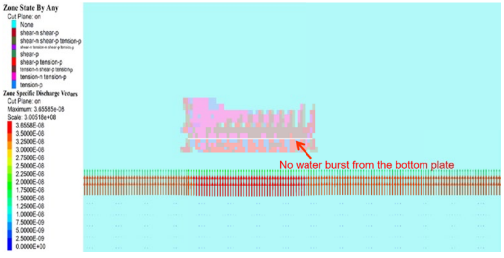

(c) Filling rate 80%

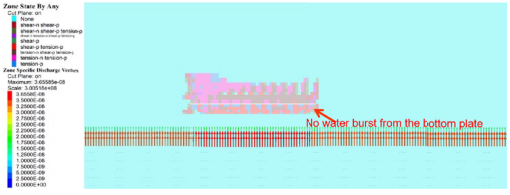

(d) Filling rate90%

Fig. 13. working face advancing 120 m, seepage vector plastic zone distribution contrast chart

5.5. Analysis of the evolution characteristics of the floor plastic zone and seepage field under different filling rates

When the working face advanced 120 m, under the conditions of confined water pressure of 2.6 MPa and filling body modulus of 0.05 GPa, under the conditions of caving method and three filling rates of 70%, 80%, and 90%, obvious water inrush occurred in the floor of the goaf under the caving method and the filling rate of 70%. The seepage vector in front of the floor of the goaf of the water inrush working face was large, becoming a strong seepage area, and the above phenomenon was stronger under the caving method. Under the filling rates of 80% and 90%, the floor of the working face was less affected by mining, and no water inrush occurred. The maximum seepage vectors were 3.6558×10-8L/s·m and 2.4043×10-8L/s·m, respectively. With the increase in filling rate, the seepage vector showed a downward trend.

During the mining process of the caving method and the filling rate of 70%, the pressure water conduction is connected with the plastic zone, the effective impermeable layer disappears, and the pressure water is conducted upward to the bottom plate along the cracks in the plastic zone, causing water inrush. The bottom plate of the working face with a filling rate of 80% and a filling rate of 90% is less affected by mining, and the height of the pressure water conduction is 5 m and 7 m, respectively. The thickness of the effective impermeable layer is 11 m and 18 m.

5.6. Linkage between vertical stress, permeability, porosity and pore water pressure of the base plate

To explore the changing rules of vertical stress, permeability, porosity, and pore water pressure in the bottom plate of confined water mining and the linkage relationship between the four. Considering that when the filling rate reaches 80% or above, the pore water pressure does not change significantly, based on the results of numerical simulation, taking the bottom plate of the working face when the filling rate is 70% as an example, the vertical stress, permeability, porosity, and pore water pressure values at different positions of the bottom plate are extracted and drawn into a linkage relationship diagram.

The relationship between the vertical stress, pore water pressure, permeability and porosity at each measuring point on the bottom plate of the working face with a filling rate of 70% is shown in Fig. 14.

As shown in Fig. 14, under the condition of 70% filling rate, the stress of the overburden strata affected by mining is transmitted to the floor through the coal wall, resulting in stress concentration. As the working face advances, the vertical stresses of the three measuring points C3, C4, and C5 reach peak values successively with the advancement distance, and the vertical stress gradually recovers with the collapse of the roof; the permeability change trend of the three points is negatively correlated with the vertical stress, because the floor is compressed to close some cracks. With the compaction of the floor, the stress of the coal wall is transferred to the goaf, and the permeability of the floor shows a recovery trend; the porosity development law of the three points is consistent, which is manifested as the floor is sheared or tensilely damaged to produce fracture zones, and the porosity of the floor increases steadily; the pore water pressure change trend of the three points is consistent, first increasing and then decreasing, and gradually stabilising.

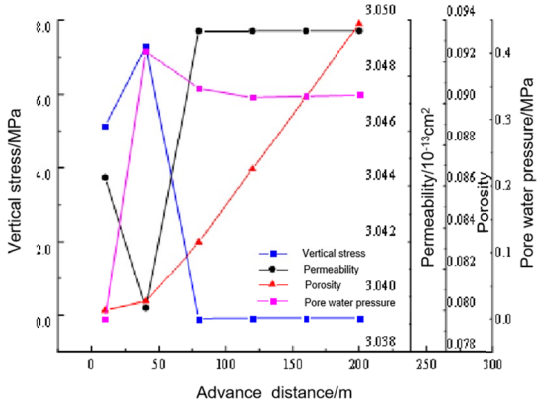

(a) C3

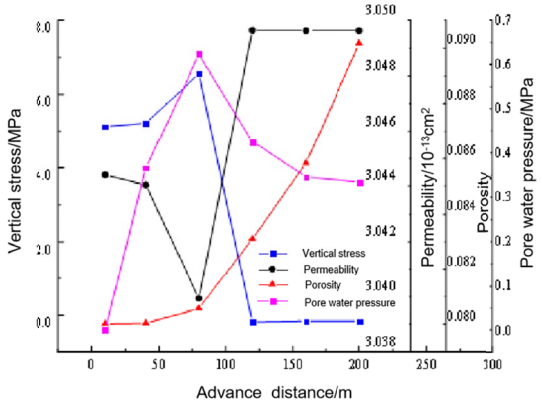

(b) C4

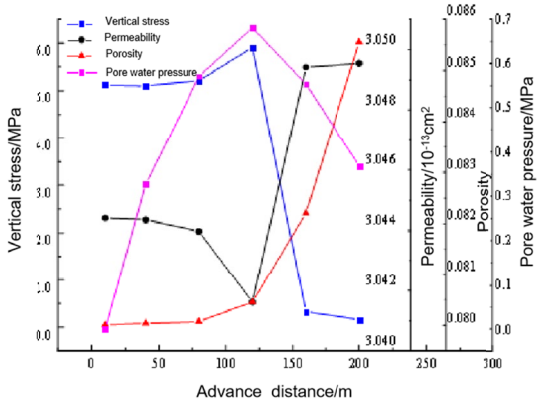

(c) C5

Fig. 14. The relationship between vertical stress, permeability, porosity and pore water pressure of different measuring points with a filling rate of 80%

6. Conclusion

This paper takes the 9101 fully mechanised mining face of a mine in the North China coalfield as the research background, and uses the superposition method to derive the formula for the maximum depth of floor damage under the action of pressurised water; the simulation is carried out through the FLAC3D finite difference software, and the software is secondary developed using the FISH language, and the formulas of volume strain, permeability, and porosity are embedded in FLAC3D. The variation law of the vertical stress, permeability, porosity, pore water pressure, and seepage field of the floor under the coupling of mining and pressurised water, as well as the linkage relationship between the vertical stress, pore water pressure, porosity, and permeability of the floor under mining above pressurised water, are studied, and the following main conclusions are obtained:

(1) The formula for the maximum damage depth of the floor in confined water mining was derived and calculated by the superposition method, and the calculation results were verified at the engineering site. Through simulation, it was found that when the working face advanced 120 m, during the caving mining and 70% filling rate mining process, the confined water was connected to the plastic zone, the effective impermeable layer disappeared, and the confined water was guided upward along the cracks in the plastic zone to the floor, causing water inrush. With the increase of the filling rate, the floor water inrush stopped, and the floor damage depth and plastic zone were significantly reduced.

(2) Backfill mining affects the permeability and porosity of the floor rock by controlling the displacement field of the floor surrounding rock, thereby reducing the formation of seepage channels and inhibiting the conduction of pressurised water. When the filling rate increases from 70% to 90%, the permeability of the floor decreases by about 45%. As the working face advances, the porosity of the floor and the Ordovician limestone water increases significantly. As the working face advances to a depth of 120 meters, the porosity in the area of the aquiclude increases. This change is linked to a rise in porosity in the upper section of the Ordovician limestone aquifer, resulting in a butterfly-shaped zone of increased porosity. When the filling rate is 80% and 90%, the porosity of the floor aquiclude is basically unchanged. Backfill mining can effectively control the porosity of the floor and improve the stability of the floor.

(3) By analysing the evolution law and linkage relationship of the vertical stress, permeability, porosity and pore water pressure of the floor in solid filling mining above confined water, it is found that the floor stress is negatively correlated with the permeability, the porosity continues to increase under the influence of mining, and the water inrush working face experiences a pore water pressure increase zone and a pore water pressure recovery zone.

Reference

[1] C. Wolkersdorfer, R. Bowell, Contemporary reviews of mine water studies in Europe, Part 2. Mine Water Environ. **24** (1), 58-76 (2005). DOI: http://doi.org/10.1007/s10230-005-0068-0

[2] P.L. Younger, C. Wolkersdorfer, Mining impacts on the fresh water environment technical and managerial guidelines for catchment scale managemnt. Mine Water Environ. **23** (1), 2-80 (2004).
DOI: http://doi.org/10.1016/j.exis.2016.10.012

[3] D. Ma, J. Wang, Z. Li, Effect of particle erosion on mining-induced water inrush hazard of karst collapse pillar. Environ. Sci. Pollutr. **26** (19), 1-10 (2019). DOI: http://doi.org/10.1007/s11356-019-05311-x

[4] J.H. Chang, J.C. Yu, Z.X. Liu, Three-dimensional numerical modeling of full-space transient electromagnetic responses of water in goaf. Appl. Geop.-Hys. **13** (3), 539-552 (2016). DOI: http://doi.org/10.1007/s11770-016-0572-y

[5] J.P. Zuo, G.S. Wu, J. Du, B. Lei, Y. Li, Rock strata failure behavior of deep ordovician limestone aquifer and multi-level control technology of water i-nrush based on microseismic monitoring and numerical methods. Rock Mech. Rock Eng. **55** (8) 4591-4614 (2022). DOI: http://doi.org10.1007/s00603-022-02891-y

[6] F. Dong, H. Yin, Q. Feng, S. Li, W. Zhou, W. Cheng, C. Jia, A new insight of water inrush mode and coal (rock) pillars setting in near-fault mining under high confined water. J. Appl. Geophys. **216**, 105136 (2023). DOI: http://doi.org10.1016/j.jappgeo.2023.105136

[7] B. Zhang, Z. Meng, Experimental study on floor failure of coal mining above confined water. Arab. J. Geosci. **12** (4), 114 (2019). DOI: http://doi.org/10.1007/s12517-019-4250-2

[8] C. Liu, P. Zhang, Y. Ou, D. Yao, Y. Tian, Analytical stress analysis method of interbedded coal and rock floor over confined water: a study on mining failure depth. J .Appl. Geophys. **204**, 104720 (2022). DOI: http://doi.org/10.1016/j.jappgeo.2022.104720

[9] W. Sun, S. Zhang, W. Guo, W. Liu, Physical simulation of high-pressure water inrush through the floor of a deep mine. Mine W-Ater. Environ. **36** (4), 542-549 (2017). DOI: http://doi.org/10.1007/s10230-017-0443-7

[10] C.J. Wang, J.G. Liu, J.X. Wang, J.W. Zhao, Y.Y. Wang, Study on floor seepage pattern of filling mining under confined water in t-he Handan-Xingtai mining area. Coal Sci. Technol. **51** (4), 140-148 (2023). DOI: http://doi.org/10.13199/j.cnki.cst.2021-0770

[11] J.G. Liu, X.W. Li, T. He, Current status and development of filling mining in coal mines in China. J. China Coal Society **45** (1), 141-150 (2020). DOI: http://doi.org/10.13225/j.cnki.jccs.yg19.1063

[12] Z.H. Li, S.L. Zhang, F. Du, Novel Experimental model to investigate fluid-solid coupling in coal seam floor for water inrush. T-Ehnički Vjesnik **45** (1), 216-223 (2018).

[13] Y. Lu, L.Wang, Numerical simulation of mining-induced fracture evolution and water flow in coal seam floor above a confi-ned aquifer. Computers and Geotechnics **67**, 157-171 (2015). DOI: http://doi.org/10.1016/j.compgeo.2015.03.007

[14] B. Zhang, Z. Meng, Experimental study on floor failure of coal mining above confined water. Arab. J. Geosci. **12** (4), 114 (2019). DOI: http://doi.org/10.1007/s12517-019-4250-2

[15] W. Mu, L. Li, Y. Zhang, G. Yu, B. Ren, Failure mechanism of grouted floor with confined aquifer based on mining-induced data. Rock Mech. Rock Eng. **56** (4), 2897-2922 (2023). DOI: http://doi.org/10.1007/s00603-022-03179-x

[16] F.D. Zhang, Study on the Lithological Effect of Mining-Induced Failure Mechanism in Coal Seam Floor. Coal Sci. Tech.-Nol. **51** (4), 166-178 (2023). DOI: http://doi.org/DOI:10.13199/j.cnki.cst.2023-0309

[17] Z. Meng, X. Shi, G. Li, Deformation, failure and permeability of coal-bearing strata during longwall mining. Eng. Geol. **208**, 69-81 (2016). DOI: http://doi.org/10.1016/j.enggeo.2016.04.029

[18] H. Ahmadi, H.A. Rasheed, Lateral torsional buckling of anisotropic laminated thin-walled simply supported beams subjected to midspan concentrated load. Compos. Struct. **185**, 348-361 (2018). DOI: http://doi.org/10.1016/j.compstruct.2017.11.027